



Article

Large Scale Laboratory Experiment: The Impact of the Hydraulic Characteristics of Flood Waves Caused by Gradual Levee Failure on Inundation Areas

Kwang Seok Yoon ¹, Khawar Rehman ², Hyung Ju Yoo ³, Seung Oh Lee ³  and Seung Ho Hong ^{4,*} 

- ¹ Department of Hydro Science and Engineering Research, Korea Institute of Civil Engineering and Building Technology, 283 Goyangdae-ro, Ilsanseo-gu, Goyang 10223, Korea; ksyoon@kict.re.kr
- ² Department of Civil Engineering, Ghulam Ishaq Khan Institute of Engineering Sciences and Technology, Topi, Swabi 23460, Pakistan; khawar.rehman@giki.edu.pk
- ³ Department of Civil and Environmental Engineering, Hongik University, Seoul 04006, Korea; hyungzu11@gmail.com (H.J.Y.); seungoh.lee@hongik.ac.kr (S.O.L.)
- ⁴ Department of Civil and Environmental Engineering, Hanyang University, Ansan 15588, Korea
- * Correspondence: sehong@hanyang.ac.kr; Tel.: +82-031-400-5143

Abstract: As a levee failure and the consequent flooding cause significant financial losses and sometimes human casualties, they have led to considerable concern among city officials. Therefore, researchers have devoted considerable effort to investigating the hydraulic characteristics of sudden transient flow in the form of propagated waves to inundation areas during a levee and/or dam failure. A large number of studies, however, have mostly focused on simple one-dimensional cases investigated numerically and/or experimentally, and thus, important hydraulic characteristics, particularly near the failure zone, have not been adequately captured because of three-dimensional complexities. Taking these complexities into consideration, this study conducts a large-scale experiment to examine the characteristics of wave propagation in an open area caused by a gradual levee failure. From the experimental observations, this study provides the propagation speed of a wave front and suggests a formula for the maximum flood depth corresponding to the peak flood wave in the inundation area. We expect the findings to provide hydraulic engineers and scientists with fundamental insights into transient flow during a gradual levee failure. By contributing to our theoretical understanding, the measurements can also be used as validation tools for future numerical simulation and are likely to contribute to the establishment of emergency action plans that can help city officials cope with flood inundation.

Keywords: flood risk; large scale experiment; levee failure; wave propagation



Citation: Yoon, K.S.; Rehman, K.; Yoo, H.J.; Lee, S.O.; Hong, S.H. Large Scale Laboratory Experiment: The Impact of the Hydraulic Characteristics of Flood Waves Caused by Gradual Levee Failure on Inundation Areas. *Water* **2022**, *14*, 1446. <https://doi.org/10.3390/w14091446>

Academic Editors: Stefano Morelli, Veronica Pazzi and Mirko Francioni

Received: 6 April 2022

Accepted: 27 April 2022

Published: 30 April 2022

Publisher's Note: MDPI stays neutral with regard to jurisdictional claims in published maps and institutional affiliations.



Copyright: © 2022 by the authors. Licensee MDPI, Basel, Switzerland. This article is an open access article distributed under the terms and conditions of the Creative Commons Attribution (CC BY) license (<https://creativecommons.org/licenses/by/4.0/>).

1. Introduction

A levee is an elongated, naturally occurring ridge or artificially constructed fill or wall that regulates water levels to prevent the overflow of a river [1]. It is often parallel to the course of a river in its floodplains or along low-lying coastlines. As they allow easier access to water resources and benefit transportation along the levee, many large cities have historically been located near levees, and this trend continues. As a result of population growth and industry demand, cities have constructed a number of levees since the late 1970's. Nevertheless, despite their importance to the greater benefit of humans and as a viable solution to reducing flooding, if levees are the last line of defense against floods [2], unexpected rising water levels by heavy rain and ensuing flood danger caused by levee failure can lead to a catastrophic impact on people, infrastructures and the economy [3]. Several examples of such events have been alarming and disastrous. In 2005, Hurricane Katrina in New Orleans, Louisiana, in the U.S. caused \$135 billion dollars in damages and 1500 fatalities [3]. More recently, in May 2020, a series of dam and levee failures by flooding in mid-Michigan caused over \$200 million in damages, and

approximately 11,000 residents were hurriedly evacuated ahead of the flooding [4]. In 2003, in Korea, Typhoon Maemi damaged over 3000 hydraulic infrastructures, including levees and bridges, where the repair cost exceeded \$4 billion. Recently, the National Disaster Management Research Institute of Korea [5] classified levees as among the most vulnerable hydraulic infrastructure during flooding. Even more worthy to note is that, in the face of recent climate change and aging infrastructures, together with growing, densely populated areas next to levees, the importance of the hydraulic and hydrologic behavior of water in case of levee failures accompanied by their reinforcement techniques have captured the spotlight in hydraulic, geotechnical, and water resources' research communities.

When a levee fails, large volumes of water enter through the opening at a very high speed within a very short time, and the momentum of the water transforms into flood waves that pour into inundation areas. Therefore, to identify areas at risk of flooding due to a levee failure and to establish an emergency action plan in response, risk management teams must understand the characteristics of flood wave propagation. Representing the physical characteristics of the flood waves by using simple kinematic wave equation, however, is challenging. After all, large scale geometric factors [6–9] as well as small scale local flow factors (i.e., non-hydrostatic pressure distribution and local turbulence effect close to the levee opening [10–12]) are required factors with which researchers are able to more accurately estimate wave propagation.

To determine the physical mechanisms of the development of flood waves caused by a levee failure and the resulting impact on inundation areas, researchers have devoted significant effort to the study of the phenomena. Because of the rapid development of mathematical power, the application of computational fluid dynamics (CFD) has become more widespread. Studies have applied one dimensional [13–15] and two-dimensional [16–18] numerical models whose overall effectiveness and reliability have shown acceptable results [7,19]. As the numerical models, however, are based on shallow water (or Saint-Venant) equations, they are not able to detect some important hydraulic characteristics, particularly those close to the opening area, because sudden transient flow near a structure leads to a unique flow field that cannot be reproduced under hydrostatic assumption, as the assumption is in a shallow water equation. Furthermore, the variation in the flow components caused by a levee failure are complex and three-dimensional. Recently, with the help of advanced computing technology, a number of researchers and engineers have focused their attention on three-dimensional dam/levee break(failure) flow simulation. Larocque et al. [11] used large-eddy simulation, coupled with k - ϵ models, to simulate abrupt dam break flow. Zhang et al. [12] applied a three-dimensional, unstructured mesh finite element model and successfully reproduced the flow field along an L-shaped open channel after a dam-break. Upon closer investigation, however, recent studies have revealed that numerical uncertainty, arising from time and spatial discretization errors, erroneous conditioning, and convergence and accuracy issues, continues to be a principal shortcoming related to CFD, leading to inconsistent results from computations and reality [20–22].

In laboratory experiments, Lauber and Hager [23], using a 14-m long, 0.5-m side rectangular flume, found significant features of dam-break flow propagating into a horizontal dry bed. In their experiments, they initiated the dam-break flow from an upstream reservoir of the flume by removing a vertical gate quickly and then measured the depths of local flow and the velocities of a wave front transferred into the downstream dry bed through the flume. From their measurements, they introduced a dimensionless coordinate in flow direction (y^*) that accounted for a combined effect of the upstream reservoir length in flow direction (L_0) and the distance from the gate along flow direction (y), suggesting the relationship between maximum wave height (h_{max}) and the dimensionless coordinate, y^* , as in the equation below.

$$\frac{h_{max}}{h_0} = \frac{4}{9} \left(1 + y^{*-1}\right)^{-5/4} \quad (1)$$

$$y^* = \lambda_0 \left(\frac{y}{h_0} \right)^{-2/3} \quad (2)$$

where h_0 is the initial water depth in the reservoir before the dam-break and λ_0 is the non-dimensional value for relative reservoir length ($= L_0/h_0$). As shown in Equation (1) and (2), the maximum wave height during the course of propagation is directly related to the relative length of the reservoir (λ_0) and the relative location in flow direction (y/h_0). Lauber and Hager [23] also found that the maximum value of the wave height approached asymptotically to the value of 4/9, which is consistent with the findings of the analytical solution in Ritter [24]. Later, other studies conducted laboratory experiments to find the effect of varied roughness in the inundation areas with and without scaled buildings within the inundation area [8,19,25,26]. Their results were used for the validation of numerical models. In more recent dam-break experiments, Issakhov and Zhandaulet [27], Khoshkonesh et al. [28], Kocaman et al. [29], and Fent et al. [30] showed the initial wave water height to be an important factor in the impact pressure induced by a wave, using digital image processing techniques and ultrasonic transducers devices to measure the hydraulic parameters. Their results showed that the wave front velocity declines as the bed friction increases, but is also significantly affected by the channel evolution and bed mobility.

As shown in the previous paragraphs, numerical models have been executed continuously, but, as explained in the previous paragraph, uncertainty issues should be addressed. Furthermore, existing empirical research was performed mainly in a small scale straight rectangular channel that can be used only as a validation tool of a numerical simulation developed based on the shallow water equation. Akanbi and Katopodes [31], Castro-Organ and Chanson [10], and Han et al. [32] mentioned that the front positions and velocities of a wave propagated into an open area without any flow restrictions and the peak water depths corresponding to various amounts of discharge are the key variables explaining the wave characteristics caused by a levee failure. In addition, Cunge and Holly [33] and Lai et al. [25] suggested that the speed of the peak propagation and the shape of the stage hydrograph are important factors for the calibration of the wave propagation numerical model. Thus, in this study, we conducted experiments in a large outdoor test basin and generated waves through various sizes of opening caused by levee failures. During the experiment, we measured the speed/shape of the wave and the depth of the water propagating into a large open area. To overcome possible flaws stemming from the scale effects under various sizes of openings of the (failure) area, we used a 30-m long by 30-m wide large outdoor test basin. From the measurements, we quantified the characteristics of wave propagation near the failure zone and derived a presumptive equation to forecast the maximum water depth over time in order to use the equation as a validation tool for numerical models of flood hazard maps [34], used for establishing risk management and evacuation plans. Furthermore, the compiled dataset in this study can be used to validate future numerical models.

2. Methods

2.1. Experimental Setup

As Figure 1a shows, we designed an entire experimental basin on a 30-m long by 30-m wide rectangular outdoor space. We constructed an inundation area, a channel for the water supply, and a levee structure within a large basin at the Korea Institute of Civil Engineering and Building Technology (KICT) in Goyang, Korea [2]. The 25-m long, 30-m wide horizontal inundation area had open boundaries on all sides in which the transitional flow generated by the gradual levee failure could freely propagate without any interference. A 30-m long, 5-m wide channel was aligned with one end of the inundation area. The channel bottom elevation was 0.4 m lower than the invert of the inundation area to store enough volume of water for the experiment, and two centrifugal pumps supplied water from large underground sumps to the channel. To reproduce a levee in the experiments, we installed a 0.6-m high and, 30-m long vertical seclusion wall along the channel and determined the height of the wall based on field measurements in Korea, which showed an

average levee height of about 10% of the channel width [35]. In the middle of the seclusion wall, we installed sliding, opening gates to simulate a gradual levee break. Lee and Han [35] found that the width of an opening during a levee failure in Korea varies around one to three times as high as the levee, or 1/8 to one time as high as the channel width. Singh and Snorrason [36] and MacDonald and Langridge-Monopolis [37] also suggested that an average width of the failure zone in case of a dam-break varies from two to five times large as the height of the dam. Thus, using a variable motor attached to the sliding opening gates to the levee, we adjusted the values of the opening width, with maximum bottom width of the opening (failure) of 3 m. The shape of the opening (failure) area also varied depending on the geotechnical properties of the levee and the flow conditions of the failure. The opening is generally classified into a rectangular or trapezoidal shape. The term ‘failure’ is defined as the inability to achieve a defined performance threshold [2]. In the case of levees, failure is initiated by the deterioration-process over time during large flooding, such as overtopping and/or erosion by hydraulic loading, and then total breach by geotechnical instability. Geotechnical instability of a levee is outside the scope of this paper, but we used the trapezoidal (1V:0.3H) shape of an opening, assuming that the deterioration process is initiated from the overtopping and leads to a total trapezoidal shape breach in the end. The trapezoidal-shaped opening area used in the experiment appears in Figure 1b.

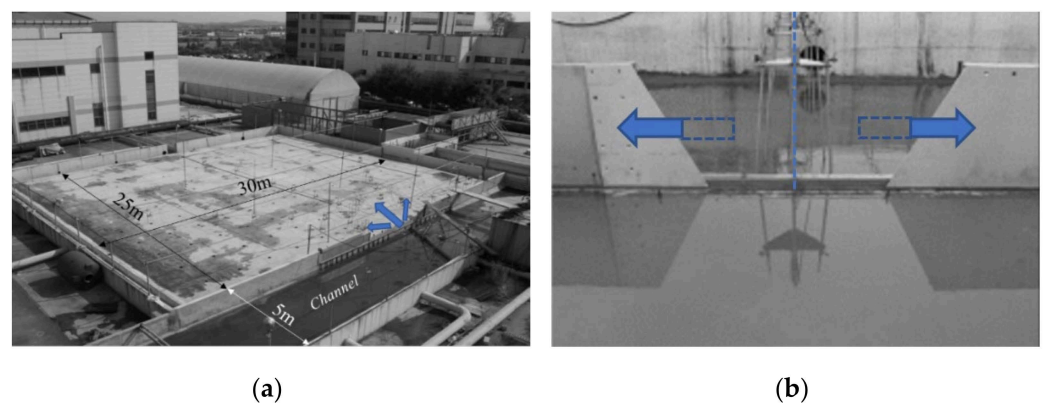


Figure 1. Experimental basin (a) and shape (b) of the opening (failure) area.

2.2. Experimental Conditions

We suggest the following variables, also shown in Figure 2, are important to an understanding of the characteristics of wave propagation: wave position (y); wave front speed (v_f); bottom opening (failure) width (B); inflow channel width (L_0); the water depth during the course of wave propagation (h); and the initial water depth over the opening (failure) area (h_0). Because the transitional flow into the inundation area is fast moving and unsteady, a conventional technique, such as use of a point gauge, cannot be used for measuring chronological changes in the water depth during propagation. Thus, we installed capacitive wave height meters, which are popularly used for ocean engineering, to measure the water depth continuously over time and to detect the arrival time of the leading edge of ocean waves within the inundation area. To illustrate the wave propagation phenomenon, Figure 2 displays the locations of the wave height meters in the basin (along a line perpendicular to the opening ($\theta = 90^\circ$) and along two diagonals ($\theta = 45^\circ$ and 135°)). We measured additional water depths close to the opening area to determine the elevation of the water surface during the failure within the channel.

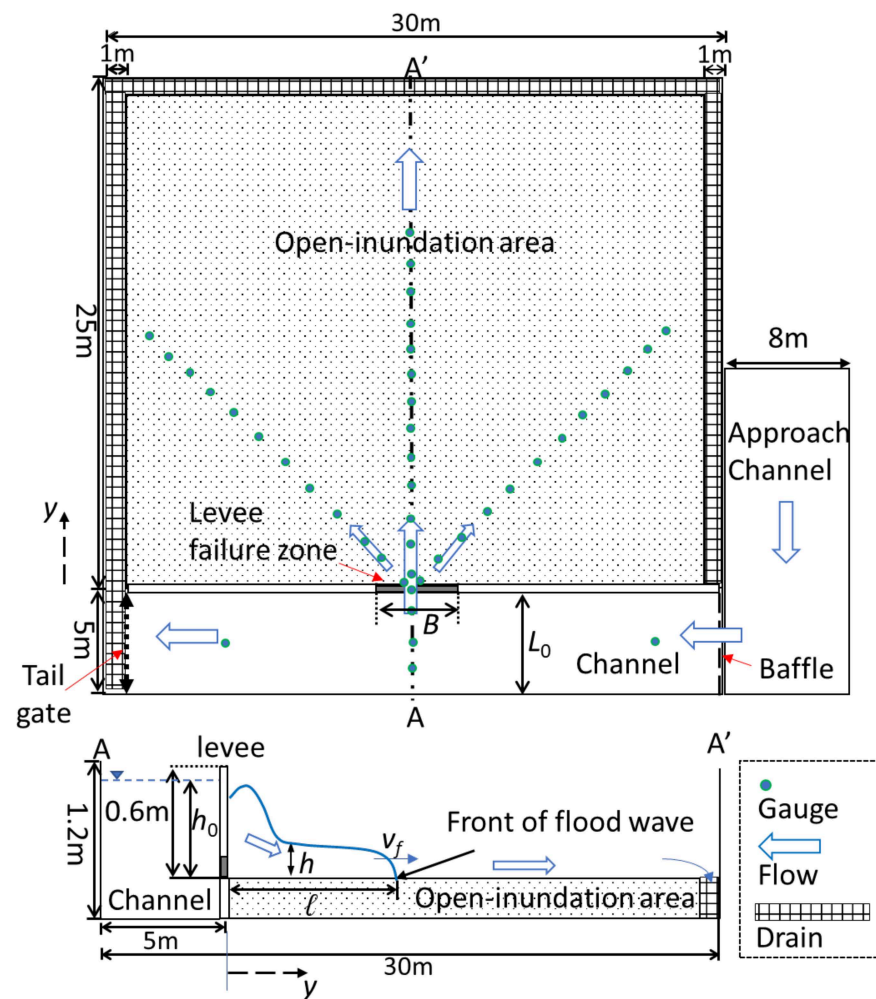


Figure 2. A schematic diagram of levee failure experiment.

At the beginning of each experiment, we raised the position of the tail gate to its maximum height and then slowly filled the channel with water until it reached the target water depth over the opening (failure) (h_0). Once the h_0 had stabilized with the target value, we did not supply the flow in the channel and initiated each experiment by gradually sliding the opening gate laterally. We tested six different sizes of bottom opening widths (B : varying from 0.5 m to 3.0 m in the interval of 0.5 m) and set the overflow depth (h_0) at intervals of 0.05 m that varied from 0.3 m to 0.55 m. In general, the levee failure flow is assumed to be instantaneous if the gate openings are within $0 \leq t_r \leq 1.25\sqrt{z/g}$ (where t_r is the removal time, z the upstream water-depth, and g gravitational acceleration) [38]. Based on the experimental conditions, the determination of the gate opening time of $0 \leq t_r \leq 0.3$ was instantaneous. Thus, to ensure a gradual levee failure, we determined that the speed of the gate opening controlled by the attached motors was 0.18 m/s. The range of experimental parameters are summarized in Table 1. The chosen minimum value of h_0 is satisfied by the recommendation of Bos [39], who showed that to eliminate surface tension as well as viscous effects, the minimum value of the water depth over a model structure should be 0.07 m. In addition, Lauber and Hager [23] found that the effects of scale are insignificant when $h_0 > 300$ mm. Flow depths in the model are generally greater than 0.07 m, which is another criterion for avoiding the effects of surface tension manifested by capillary waves in free-surface flow models [40].

Table 1. Ranges of experimental parameters.

Width of the Bottom Opening, B (m)	Shape of the Failure *	Initial Head over the Opening, h_0 (m)	Width of the Channel, L_0 (m)	Speed of the Failure, (m/s)
0.5, 1.0, 1.5, 2.0, 2.5, 3.0	Trapezoidal 1V:0.3H	0.30, 0.35, 0.40, 0.45, 0.50, 0.55	5	0.18

* V indicates vertical and H indicates horizontal.

3. Results

3.1. Speed of the Wave Front

To find the hydraulic characteristics of the wave front generated by a gradual levee failure, we observed the chronological locations of the leading edge of the flood wave in the course of propagation and their extension phenomena. Figure 3a illustrates the location of wave front (y) from an opening over time, measured along the perpendicular (open symbol) and diagonal ($\theta = 45^\circ$; closed symbol) directions with respect to different values of initial head (h_0) in the case of $B = 1.0$ m. As the acceleration of the flow was strong through the levee failure due to gravity and then decelerated in the open area and faster moving over the failure adjacent to the slower moving flow in the channel, it induced a complex interaction that included the strong transverse transfer of the longitudinal momentum from the levee to the open area. We observed this phenomenon in the gradual decrease of the slope of wave front position vs time curve, shown in Figure 3a, because the relative effect of momentum transfers according to the speed of the wave front, which is the maximum proximity to the failure zone and then becomes smaller over time as a result of the friction induced by bed roughness within the dry open area. Furthermore, as shown in Figure 3a, in the case of higher h_0 , the wave front propagates further along the perpendicular direction than in the diagonal direction. Thus, the speed at the leading edge of flood wave (v_f) along the perpendicular direction shown in Figure 3b was estimated using the data shown in Figure 3a. As the “golden time”, which is the minimum time required for people to evacuate from a natural disaster, following an evacuation order immediately after a levee failure, is related to the speed of the flood wave in the inundation area, the speed of the wave front during a levee failure is a critical variable that signals the need for preparing a safety zone within the lowland. As shown in Figure 3b, the v_f increases close to the failure because of higher momentum/energy transfer from the vertical gravity-dominant deep water (potential energy) to shallow water (kinetic energy), flowing in a pan shape in the radial direction. Then, the speed decreases as the wave propagates further from the failure.

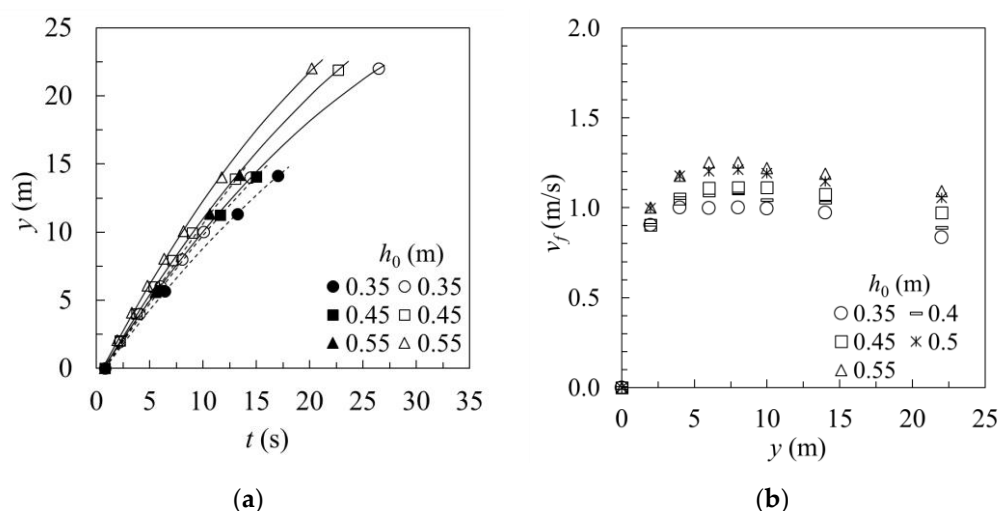


Figure 3. Propagation of the wave front over time (a) and the wave front speed (b) with respect to different values of the initial head over opening (h_0) for $B = 1.0$ m case.

3.2. Morphological Characteristics of the Flood Wave

To analyze changes in the flood waveform during propagation, we plotted the chronological changes in the waveform measured along $\theta = 90^\circ$ in terms of non-dimensional variables in the case of $h_0 = 0.55$ m and $B = 1.0$ m over non-dimensional time $T (=t \times \sqrt{g/h_0})$ expressed in initial water depth over the opening area (h_0), gravitational acceleration (g) and time after levee starts to fail (t), depicted in Figure 4. The dimensionless time $T = 0$ refers to the initiation of the levee failure. As shown in the Figure, as soon as the levee starts to fail, the wave height quickly begins to increase, reaching a maximum within a short period of time; then it begins to decrease slowly over time in each wave form at different locations. It is interesting to note that the peak value of the height of each form decreases quickly as the distance from failure y increases, the result of friction induced by the dry bed, different from the wave propagation along a one-dimensional channel [23,41]. Analogous to wave propagation initiated by a dam-break within a horizontal rectangular channel bed, the rapid propagation of a wave is accompanied by severe elongation of the air and water interface along a constrained channel in one direction and the rapid conversion of potential energy into kinetic energy [42]. In the current experiment, however, the wave propagated into the open space in all radial directions, leading to a more rapid decrease in the height of the peak wave.

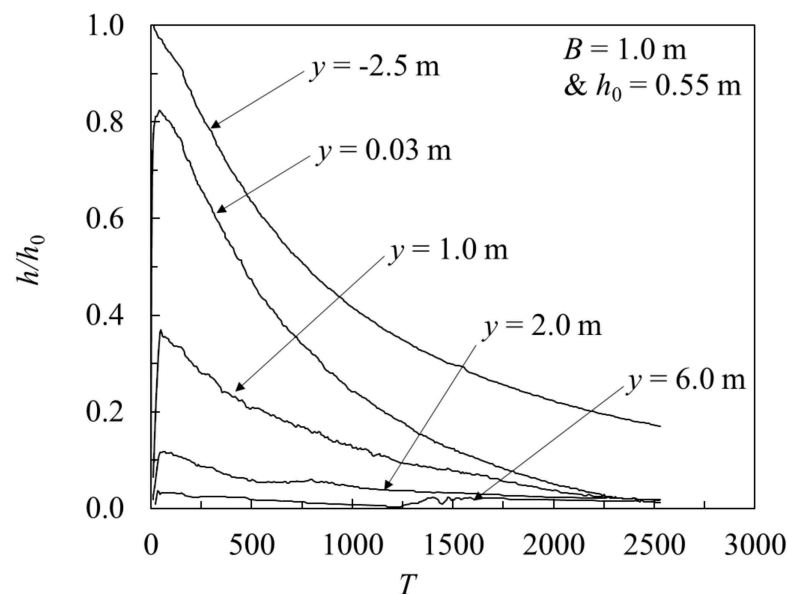


Figure 4. Chronological changes in the flood waveform with respect to various locations, y , measured along $\theta = 90^\circ$ (cases with $h_0 = 0.55$ m and $B = 1.0$ m).

In addition to the chronological changes in flood waveform during the course of wave propagation, Figure 5 shows the effect of the failure width on the morphological characteristics of a flood wave measured at two different locations with respect to different values of B . As shown in Figure 5a, the wave height quickly increases and then decreases gradually after a short period of time for the cases measured at $y = 0.03$ m along $\theta = 90^\circ$. The peak value of the non-dimensional wave height (h/h_0) in each waveform appears to have a corresponding value in Figure 5a (about 83% of h_0), even in cases with different failure widths because the wave height close to the failure area reached a maximum before the gates were fully opened under the assumption of a gradual levee failure. We found, however, that the peak value of h/h_0 decreased as B decreased further away from the failure zone, and the reduction rate became higher as the B decreased as they propagated, as shown in Figure 5b. Depending on the failure width, the amount of inflow into the inundation area varied. In addition, as the failure width increased, the smaller reduction in the peak wave height resulted in a higher “flood intensity” in the inundation area. Thus, in

the case of a levee failure, minimizing the bottom width of the failure is critical in order to reduce the intensity of the inundation.

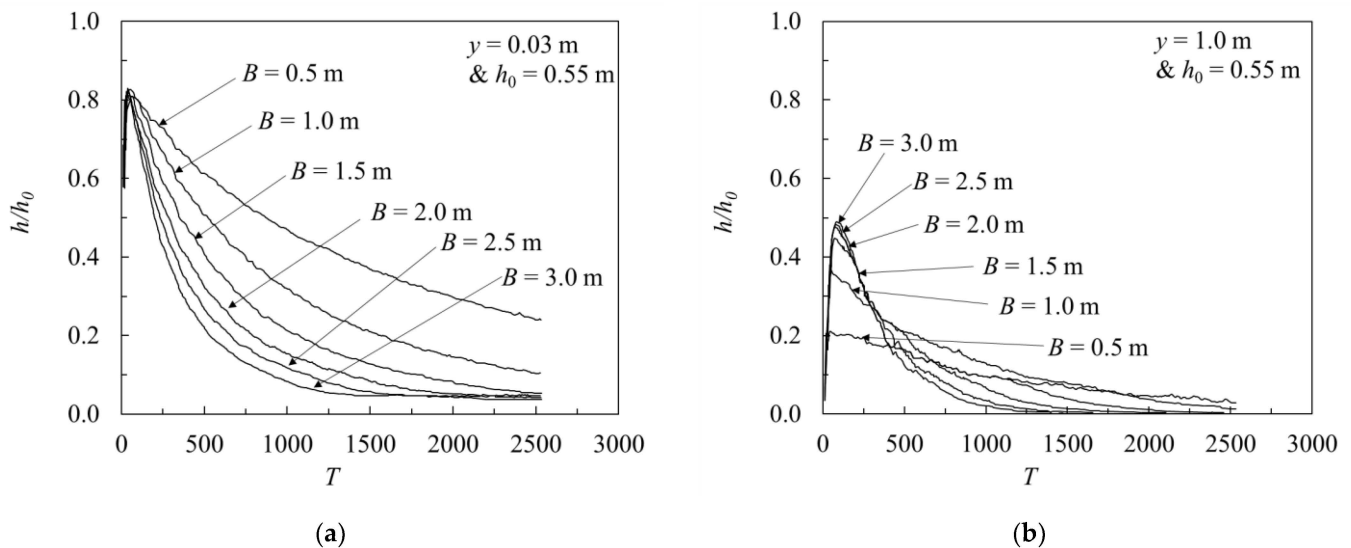


Figure 5. Morphological characteristics of a flood wave with respect to different failure widths, B , at two locations: (a) $y = 0.03$ m and (b) $y = 1.0$ m along $\theta = 90^\circ$.

To find the effect of initial head h_0 over opening on the wave form, we analyzed the morphological characteristics of flood wave, shown in Figure 6, with respect to different initial heads measured with $B = 1.0$ m along $\theta = 90^\circ$. As shown in Figure 6a, as the h_0 decreases, the peak value of h/h_0 also slightly decreases close to the failure zone, but the effect of h_0 is not significant to the peak value of h/h_0 as the wave propagates, as shown in Figure 6b. Furthermore, as shown in Figure 6, based on the findings that the shapes of the morphological characteristics of a flood wave are similar, the effect of h_0 on the shape of wave formation is insignificant during a gradual levee failure.

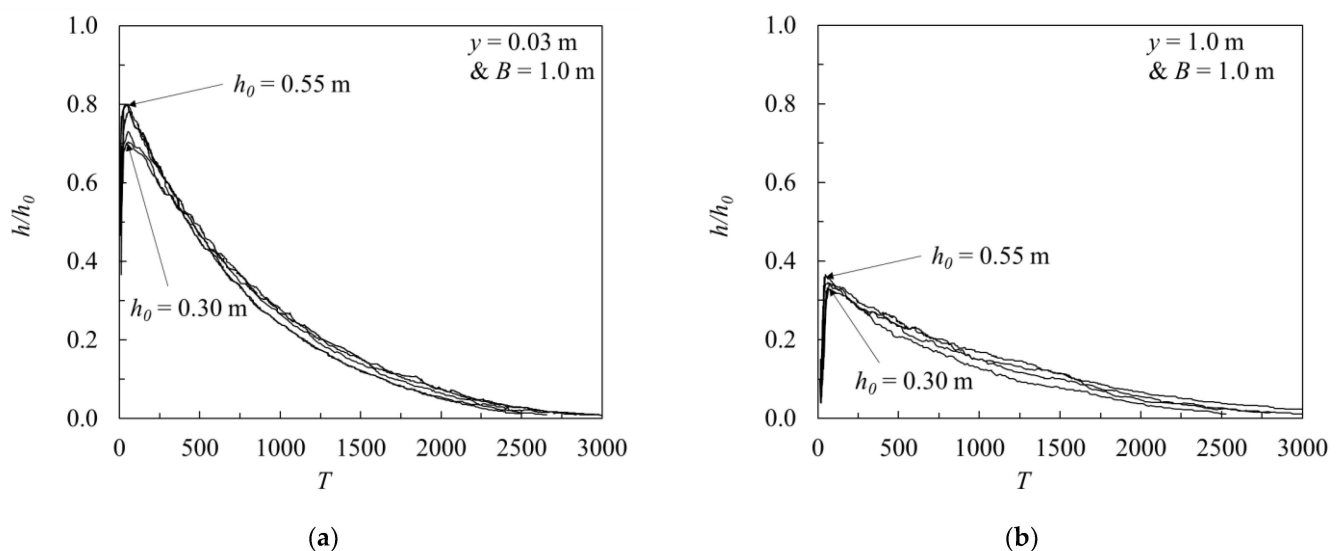


Figure 6. Morphological characteristics of the flood wave with respect to the initial head h_0 over the opening at two different locations: (a) $y = 0.03$ m and (b) $y = 1.0$ m with $B = 1.0$ m measured along $\theta = 90^\circ$.

4. Discussion

As shown in Figure 3, the propagation of a wave is transient and non-uniform with a large spatial and temporal gradient. Thus, to understand the evolution of the speed of

a wave front in more depth, we normalized the speed of the leading edge (v_f) according to the reference wave speed, ($\sqrt{gh_0}$), and calculated the non-dimensional time as T ($=t \times \sqrt{g/h_0}$) [24,42]. Figure 7 shows the evolution of the wave front speed during its propagation in terms of the non-dimensional parameters, V_f and T . As shown in Figure 7, V_f rapidly increases during the initial stage. The Figure also shows that as T increases, however, a transition point at a certain dimensionless time (T is about 20 at that point) occurs. In addition, the velocity of the wave front, which is sub-critical, is smaller than the reference wave speed, $\sqrt{gh_0}$. In all cases, because of propagation into the three-dimensional open dry space, the velocity of the wave front was smaller than that found by the analytical solution in Ritter [24], who identified propagation in a one-dimensional space. From the data shown in Figure 7, we used least-squares regression to analyze the measured distribution of the dimensionless velocity over time and found that it is closely agreed with the following best-fit equations, in which the dimensionless velocity has a unique power function of the dimensionless time.

$$V_f = 0.221 T^{0.314} \text{ when } T < 20 \quad (3)$$

$$V_f = 0.730 T^{-0.087} \text{ when } T > 20 \quad (4)$$

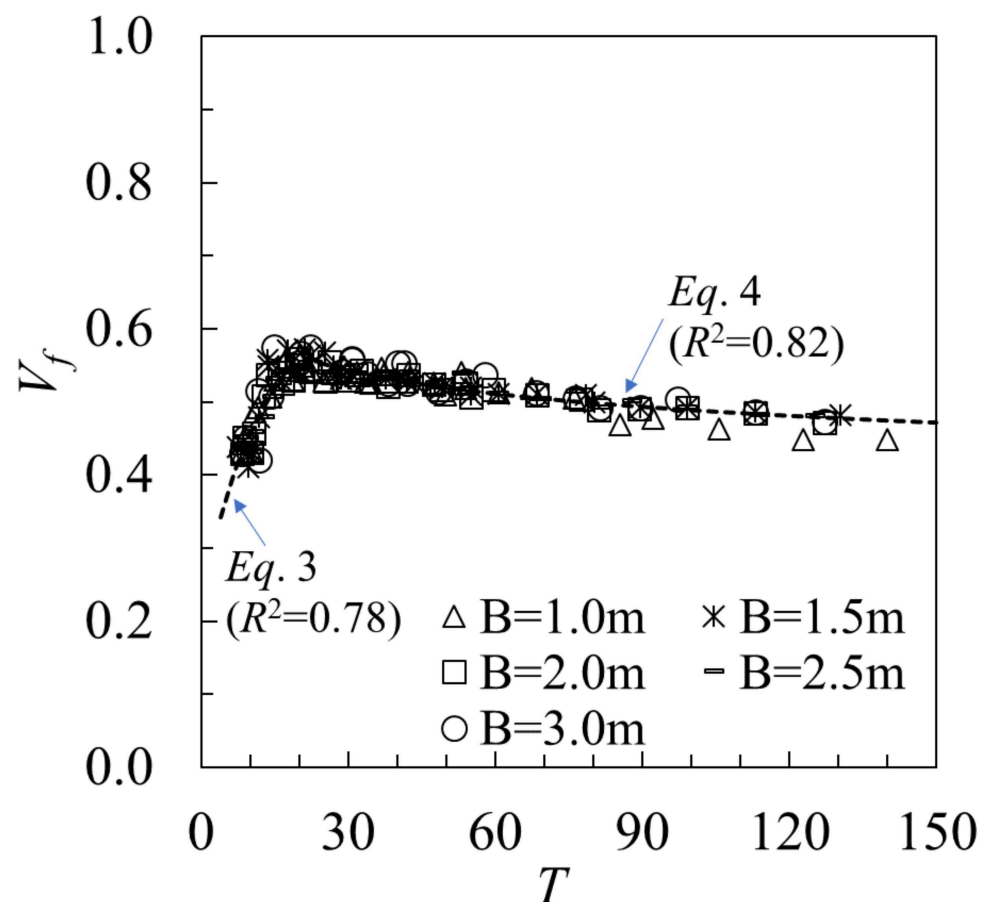


Figure 7. Evolution of the dimensionless wave front speed V_f over dimensionless time T .

As explained in the Introduction, in a laboratory flume experiment, Lauber and Hager [23] found a relationship between the wave height propagated into a horizontal dry bed during a dam-break and the dimensionless coordinate in flow direction, y^* . Thus, in this section, we compare results from the current experiments to those conducted by Lauber and Hager [23]. Figure 8a shows the tracking propagation of the relative maximum wave height conducted under different failure widths, but with $h_0 = 0.55$ m. Figure 8a

shows that the non-dimensional value of the maximum wave height increased quickly when $y^* < \sim 5.0$ and then gradually increased over the course of propagation instead of approaching to the value of $4/9$ as in Equation (1). Furthermore, the magnitude of h_{max}/h_0 was less than the magnitudes suggested by Lauber and Hager [23] when $0 < y^* < \sim 5.0$. A possible explanation for this finding is that the dam-break scenarios in which Lauber and Hager [23] simulated vertical dam-breaks but gradual lateral levee failures along a river, similar to those in our experiments, led to a formation of the initial shape of a flood wave that differed from ours. Furthermore, the power relationship between h_{max}/h_0 and y^* was not unique because the water depth travelling radially to an open space decreased more quickly than a flood wave travelling in a one-dimensional waterway, as found by Lauber and Hager [23]. Referring to the experimental results conducted with an identical failure bottom width ($B = 1.0$ m), we explored the effect of overflow depth (h_0) on the propagation of h_{max}/h_0 , shown in Figure 8b. In the Figure, the maximum wave height shows trends similar to those in Figure 8a. It is interesting, however, to note that within the lower range of y^* ($y^* < 10$), the effect of h_0 on h_{max}/h_0 is negligible. After all, the morphological characteristics of a flood wave are nearly independent of the value of h_0 close to the failure, as explained in the previous paragraph. Further away from the failure zone, however, h_{max}/h_0 increases as h_0 increases.

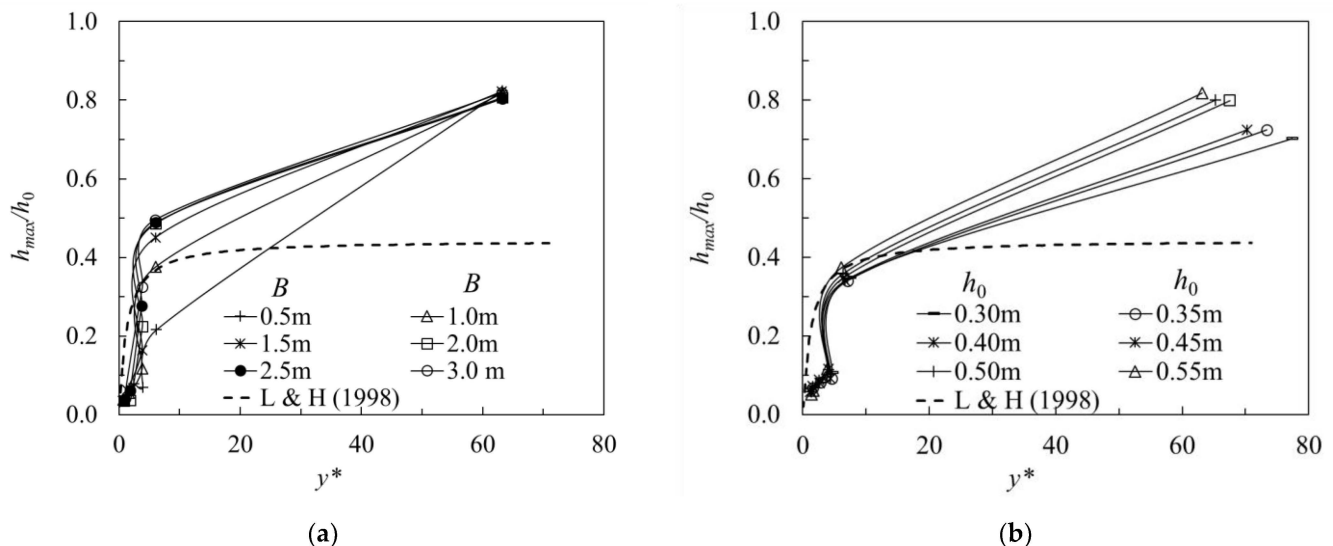


Figure 8. Comparison between the experimental results in this paper and those in Lauber and Hager [23] with respect to the different failure widths (a) and the initial head over the failure (b).

In the case of an inundation caused by a levee failure along a river, as the flow moves in a radial direction toward an inundation area, application of the non-dimensional variable, y^* , developed in a one-dimensional waterway [23] was not appropriate. Furthermore, unlike the flow from a dam-break, the flow from a levee failure is supplied to the inundation area continuously from a river after the failure, so the effect of the relative reservoir length cannot be determined. Accordingly, in this experiment, we set the bottom width of the levee failure as the governing length variable, which affected the maximum wave height in the inundation area. Figure 9 illustrates the relationship between non-dimensional variables h_{max}/h_0 and y/B by reflecting the characteristics of the maximum wave height; that is, it is proportional to the bottom width of the levee failure, and in inverse proportion to the distance from the levee failure area. The measured distribution of the dimensionless maximum wave height shows the unique power function of the y/B and closely agrees with the best-fit equations, Equation (5) ($R^2 = 0.87$):

$$\frac{h_{max}}{h_0} = \frac{4}{25} \left(\frac{y}{B} \right)^{-2/5} \quad (5)$$

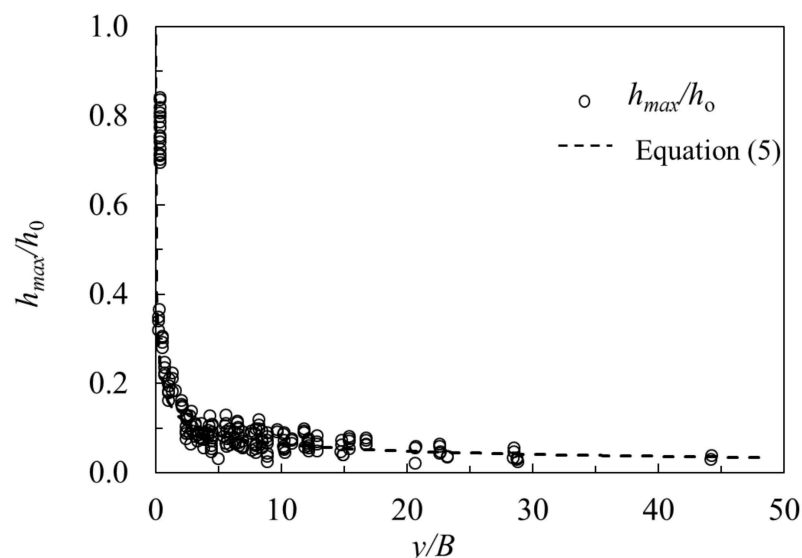


Figure 9. Relationship between relative propagation distance (y/B) and maximum wave height (h_{max}/h_0).

The results that appear in Figure 9 show the phenomena of the abrupt reduction of the maximum water depth when the wave travels from the levee failure area. Although the effect of boundary roughness was small during the initial wave propagation, it had a significant effect for large times. Moreover, the equations suggested in this study show that the maximum water depth can be predicted by reflecting physical properties using simple variables.

5. Conclusions

This paper presented the results of a large-scale experiment that sought to explain the characteristics of a flood wave within a dry inundation area generated by a gradual levee failure. Because of higher momentum/energy transfer during the levee failure, the velocity of the wave front increased to a certain non-dimensional time and then gradually decreased over the remaining course of the propagation. The findings showed that the speed of the leading edge, normalized by the reference wave speed, had a unique power relationship with the non-dimensional time suggested by Ritter [24]. With regard to the morphological characteristics of the wave, the height of the wave increased quickly and reached a similar value of h_{max}/h_0 regardless of the bottom width (B) during the gradual failure; further away from the levee, however, h_{max}/h_0 increased as B increased, and the influence of the overflow water depth (h_0) on h_{max}/h_0 decreased as the distance from levee failure area increased. From these findings, we concluded that B is a strong control variable with respect to risk management, therefore, minimizing the failure's bottom width (B) in order to reduce inundation intensity is necessary. Finally, to forecast changes in the maximum water depth of the inundation, we derived an empirical equation that helps to clarify the inundation range and chronological changes in a space-time dimension. Although the empirical equation is derived based on the laboratory experiment using an artificial levee failure having the highest initial water depth of 0.55 m, the equation can serve as a validation tool for numerical models of flood hazard maps used for establishing evacuation plan in the event of a possible levee failure. The study also showed that the first moments during the failure of a levee involved severe transient flow of high velocity and a considerable impact of waves on structures within the inundation area. The type of flow, however, will differ depending on a number of conditions. Thus, if additional experiments on the characteristics of a flood wave are conducted under different geotechnical properties of levees and various roughness elements within an inundation area, such experiments should help clarify the characteristics of a flood wave caused by a levee failure. In such

a case, useful data will enhance the ability of city officials to establish emergency action plans and prepare flood inundation maps.

Author Contributions: K.S.Y. and S.O.L. designed experiments and measured the laboratory results; H.J.Y., K.R. and S.H.H. analyzed the data and interpreted the results; S.O.L., H.J.Y., K.R. and S.H.H. prepared the manuscript; and all authors reviewed and edited the manuscript. All authors have read and agreed to the published version of the manuscript.

Funding: This work was supported by a Grant (127568) from the Water Management Research Program funded by Ministry of Environment of Korean government. In addition, the corresponding author gratefully appreciated the start-up support from Hanyang University ERICA.

Institutional Review Board Statement: Not applicable.

Informed Consent Statement: Not applicable.

Data Availability Statement: Not applicable.

Conflicts of Interest: The authors declare no conflict of interest.

References

1. Petroski, H. Levees and other raised ground. *Am. Sci.* **2006**, *94*, 7–11. [\[CrossRef\]](#)
2. Lee, S.; Yoon, K.; Lee, J.; Hong, S.H. Estimates of discharge coefficient in levee breach under two different approach flow types. *Sustainability* **2019**, *11*, 2374. [\[CrossRef\]](#)
3. Alderman, K.; Turner, L.; Tong, S. Floods and human health: A systematic review. *Environ. Int.* **2012**, *47*, 37–47. [\[CrossRef\]](#) [\[PubMed\]](#)
4. Hayes, J. Mid-Michigan flooding and dam failure confirm the value of the Mackinac center. *IMPACT Mag.* **2020**, *19*.
5. Yoon, K.S. Study on behavior of flood wave front varied with levee breach speed in flat inundation Area. *J. Korea Acad.-Ind. Coop. Soc.* **2017**, *18*, 537–544.
6. Haltas, I.; Elci, S.; Tayfur, G. Numerical simulation of flood wave propagation in two-dimensions in densely populated urban areas due to dam break. *Water Resour. Manag.* **2016**, *30*, 5699–5721. [\[CrossRef\]](#)
7. Pilotti, M.; Maranzoni, A.; Tomirotti, M.; Valerio, G. 1923 Gleno dam break: Case study and numerical modeling. *J. Hydraul. Eng.* **2011**, *137*, 480–492. [\[CrossRef\]](#)
8. Shige-eda, M.; Akiyama, J. Numerical and experimental study of two-dimensional flood flows with and without structures. *J. Hydraul. Eng.* **2003**, *129*, 817–821. [\[CrossRef\]](#)
9. Soares-frazao, S.; Zech, Y. Dam-break flow through an idealized city. *J. Hydraul. Res.* **2008**, *46*, 648–658. [\[CrossRef\]](#)
10. Castro-Orgaz, O.; Chanson, H. Ritter’s dry-bed dam-break flows: Positive and negative wave dynamics. *Environ. Fluid Mech.* **2017**, *17*, 665–694. [\[CrossRef\]](#)
11. Larocque, L.; Imran, J.; Chaudhry, M.H. 3D numerical simulation of partial breach dam-break flow using the LES and *k-e* turbulence models. *J. Hydraul. Res.* **2013**, *51*, 145–157. [\[CrossRef\]](#)
12. Zhang, T.; Fang, F.; Feng, P. Simulation of dam/levee-break hydrodynamics with a three-dimensional implicit unstructured-mesh finite element model. *Environ. Fluid Mech.* **2017**, *17*, 959–979. [\[CrossRef\]](#)
13. Yanmaz, A.M.; Seçkiner, G.; Ozyaydin, V. A method for optimum layout design of concrete gravity Dams. *Int. J. Korea Water Resour. Assoc.* **2001**, *2*, 199–207.
14. Macchione, F. Model for predicting floods due to earthen dam breaching. I. Formulation and evaluation. *J. Hydraul. Eng.* **2008**, *134*, 1688–1696. [\[CrossRef\]](#)
15. Froehlich, D.C. Embankment dam breach parameters and their uncertainties. *J. Hydraul. Eng.* **2008**, *134*, 1708–1721. [\[CrossRef\]](#)
16. Brufau, P.; Vazquez-Cendon, M.E.; Garcia-Navarro, P. A numerical model for flooding and drying of irregular domains. *Int. J. Numer. Methods Fluids* **2002**, *39*, 247–275. [\[CrossRef\]](#)
17. Qi, H.; Altinakar, M. GIS-based decision support system for Dam break flood management under uncertainty with two-dimensional numerical simulations. *J. Water Resour. Plan. Manag.* **2012**, *138*, 334–341. [\[CrossRef\]](#)
18. Mahdizadeh, H.; Stansby, P.K.; Rogers, B.D. Flood wave modeling based on a two-dimensional modified wave propagation algorithm coupled to a full-pipe network solver. *J. Hydraul. Eng.* **2012**, *138*, 247–259. [\[CrossRef\]](#)
19. Soares-frazao, S.; Zech, Y. Experimental study of dam-break flow against an isolated obstacle. *J. Hydraul. Res.* **2007**, *45*, 27–36. [\[CrossRef\]](#)
20. Soares-Frazão, S.; Canelas, R.; Cao, Z.; Cea, L.; Chaudhry, H.M.; Die Moran, A.; Zech, Y. Dam-break flows over mobile beds: Experiments and benchmark tests for numerical models. *J. Hydraul. Res.* **2012**, *50*, 364–375. [\[CrossRef\]](#)
21. Roger, S.; Dewals, B.J.; Erpicum, S.; Schwanenberg, D.; Schüttrumpf, H.; Köngeter, J.; Piroton, M. Experimental and numerical investigations of dike-break induced flows. *J. Hydraul. Res.* **2009**, *47*, 349–359. [\[CrossRef\]](#)
22. Aureli, F.; Dazzi, S.; Maranzoni, A.; Mignosa, P.; Vacondio, R. Experimental and numerical evaluation of the force due to the impact of a dam-break wave on a structure. *Adv. Water Resour.* **2015**, *76*, 29–42. [\[CrossRef\]](#)

23. Lauber, G.; Hager, W.H. Experiments to dambreak wave: Horizontal channel. *J. Hydraul. Res.* **1998**, *36*, 291–307. [\[CrossRef\]](#)
24. Ritter, A. Die Fortpflanzung von Wasserwellen. *Z. Ver. Dtsch. Ing.* **1982**, *36*, 947–954.
25. Lai, C.; Liu, C.; Lin, Y. Experiments on flood-wave propagation in compound channel. *J. Hydraul. Eng.* **2000**, *126*, 492–501. [\[CrossRef\]](#)
26. Kocaman, S.; Ozmen-Cagatay, H. The effect of lateral channel contraction on dam break flows: Laboratory experiment. *J. Hydrol.* **2012**, *432*, 145–153. [\[CrossRef\]](#)
27. Issakhov, A.; Zhandaulet, Y. Numerical simulation of dam break waves on movable beds for various forms of the obstacle by VOF method. *Water Resour. Manag.* **2020**, *34*, 2269–2289. [\[CrossRef\]](#)
28. Khoshkonesh, A.; Nsom, B.; Gohari, S.; Banejad, H. A comprehensive study on dambreak flow over dry and wet beds. *Ocean Eng.* **2019**, *188*, 106279. [\[CrossRef\]](#)
29. Kocaman, S.; Güzel, H.; Evangelista, S.; Ozmen-Cagatay, H.; Viccione, G. Experimental and numerical analysis of a dam-break flow through different contraction geometries of the channel. *Water* **2020**, *12*, 1124. [\[CrossRef\]](#)
30. Fent, I.; Zech, Y.; Soares-Fraza, S. Dam-break flow experiments over mobile bed: Velocity profile. *J. Hydraul. Res.* **2019**, *57*, 131–138. [\[CrossRef\]](#)
31. Akanbi, A.; Katopodes, N. Model for flood propagation on initially dry land. *J. Hydraul. Eng.* **1988**, *114*, 689–706. [\[CrossRef\]](#)
32. Han, K.; Lee, J.; Park, J. Flood inundation analysis resulting from Levee-break. *J. Hydraul. Res.* **1998**, *36*, 747–759. [\[CrossRef\]](#)
33. Cunge, J.A.; Holly, F.M., Jr.; Verwey, A. *Practical Aspects of Computational River Hydraulics*. Pitman Pub: Boston, MA, USA; London, UK, 1980.
34. Cea, L.; Costabile, P. Flood Risk in Urban Areas: Modelling, Management and Adaptation to Climate Change. A Review. *Hydrology* **2022**, *9*, 50. [\[CrossRef\]](#)
35. Lee, J.; Han, K. A forecasting model for the flooded area resulting from breached levee. *J. Korean Assoc. Hydrol. Sci.* **1989**, *22*, 223–231. (In Korean)
36. Singh, K.P.; Snorrason, A. *Sensitivity of Outflow Peaks and Flood Stages to the Selection of Dam Breach Parameters and Simulation Models*; Final Report; Illinois Department of Energy and Natural Resources: Champaign, IL, USA, 1982.
37. MacDonald, T.C.; Langridge-Monopolis, J. Breaching characteristics of dam failures. *J. Hydraul. Div.* **1984**, *110*, 567–586. [\[CrossRef\]](#)
38. Bahmanpouri, F.; Daliri, M.; Khoshkonesh, A.; Namin, M.M.; Buccino, M. Bed compaction effect on dam break flow over erodible bed; experimental and numerical modeling. *J. Hydrol.* **2021**, *594*, 125645. [\[CrossRef\]](#)
39. Bos, M.G. *Discharge Measurement Structures*; Publication20; International Institute of Land Reclamation and Improvement: Wageningen, The Netherlands, 1989.
40. ASCE. *Hydraulic Modeling: Concepts and Practice*; ASCE Manual No. 97; ASCE: Reston, VA, USA, 2000.
41. Sturm, T.W. *Open Channel Hydraulics*; McGraw Hill: New York, NY, USA, 2001.
42. Garoosi, F.; Merabtebe, T.; Mahdi, T. Numerical simulation of merging to two rising bubbles with different densities and diameters using an enhanced Volume-Of-Fluid(VOF) model. *Ocean. Eng.* **2022**, *247*, 110711. [\[CrossRef\]](#)